Cerebral Cortex, 2025, **35**, bhaf079
https://doi.org/10.1093/cercor/bhaf079
Advance access publication date 11 April 2025
Original Article

Advanced concentrative absorption meditation reorganizes functional connectivity gradients of the brain: 7T MRI and phenomenology case study of jhana meditation

Umay Demir[1,2,3], Winson Fu Zun Yang[1,2], and Matthew D. Sacchet[1,2,*]

[1]Meditation Research Program, Department of Psychiatry, Massachusetts General Hospital, Harvard Medical School, Boston, MA 02129, United States
[2]Athinoula A. Martinos Center for Biomedical Imaging, Department of Radiology, Massachusetts General Hospital, Harvard Medical School, Boston, MA 02129, United States
[3]Faculty of Medicine, Graduate School of Life Sciences, Utrecht University, 3584 CS Utrecht, the Netherlands

*Corresponding author: Matthew D. Sacchet, Meditation Research Program, Athinoula A. Martinos Center for Biomedical Imaging, 149 13th Street Charlestown, Boston, MA 02129, United States. Email: meditationadministration@mgh.harvard.edu

There is growing scientific interest in advanced meditation, and particularly the Theravada Buddhist advanced concentrative absorption meditation known as jhana (ACAM-J). ACAM-J includes a series of eight consecutive meditative states, which are radically altered states of consciousness. The neuroscience of ACAM-J, specifically brain reorganization, remains underspecified in part due to the difficulty of finding and studying expert ACAM-J meditators and challenges related to laboratory investigation of ACAM-J. Using a nonlinear dimensionality reduction technique applied to human functional neuroimaging in an intensive case study, we investigated brain reorganization during ACAM-J. We applied linear mixed models and correlations to explore relations among brain reorganization and ACAM-J phenomenology. Results demonstrated that ACAM-J induces disruption of the hierarchical organization of the brain by shifting the gradients toward a more globally integrated rather than segregated state between sensory-related and higher-order cognitive regions. Additionally, ACAM-J induces a separation between sensory-related and attention modulation-related regions, resulting in greater differentiation in functional organization of these regions, consistent with phenomenological reports. This study highlights the need for further research into brain reorganization and health-related implications of both short-term and long-term practice of ACAM-J.

Key points/highlights

- The neuroscience of advanced concentrative absorption meditation (ACAM) has the potential to improve our knowledge of well-being and altered states of consciousness but remains underexplored due to methodological challenges.
- We investigated functional reorganization of the brain during ACAM-J using gradient analysis and demonstrated that ACAM-J disrupts the hierarchical organization of the brain during meditation.
- Additionally, we demonstrated that ACAM-J increases differentiation between primary sensory areas and areas related to attention modulation.

Keywords: advanced meditation; brain functional connectivity; gradient analysis; jhana advanced concentrative absorption meditation (ACAM-J); neurophenomenology.

Introduction

Advanced meditation, an emerging subfield within contemplative science, investigates skills, states, and stages of meditation that unfold with mastery and over time (Sacchet et al. 2024). Advanced meditation goes beyond conventional mindfulness meditation, including mindfulness for stress reduction (Sezer et al. 2022), and includes the study of meditative development, the developmental trajectory of advanced meditation states and stages, and meditative endpoints, or limits and endpoints of advanced meditation practice (Sacchet et al. 2024). Meditative endpoints are sometimes described using terms such as "awakening," "enlightenment," or "salvation" (Amaro 2021; Anālayo 2021). Recent advanced meditation research highlights the potential for meditation to foster altered states of consciousness that transcend conventional well-being, calling for a re-evaluation of the boundaries of human experience and perception (Chowdhury et al. 2023; Galante et al. 2023; Laukkonen et al. 2023; Wright et al. 2023; Ganesan et al. 2024; Van Lutterveld et al. 2024; Yang et al. 2024a).

Advanced concentrative absorption meditation (ACAM) is a class of advanced meditation that leads to psychological absorption, or full immersion in the meditation object (Sparby and Sacchet 2024; Yang et al. 2024a, 2024b). Practiced in diverse spiritual and religious traditions, ACAM shares a common goal of achieving states of altered consciousness and awareness (Louchakova-Schwartz 2011; Fisher 2022). The focus of this study

Received: September 30, 2024. **Revised:** February 12, 2025. **Accepted:** March 19, 2025

is on a Theravada Buddhist type of ACAM known as *jhana* or referred to as ACAM-J in this context.

ACAM-J consists of a series of eight rich meditative altered states of consciousness, starting from ACAM-J1, continuing up to ACAM-J8 (Brasington 2015; Sparby and Sacchet 2024; Yang et al. 2024b). See Yang et al. (2024b) and Sparby and Sacchet (2024) for in-depth discussion of ACAM-J. During the "form" ACAM-J (ACAM-J1 to ACAM-J4), the meditator is still aware of the external environment, although passively. Progressing through the "formless" ACAM-J (ACAM-J1 to ACAM-J4) systematically dissolves conventional boundaries of perception, revealing increasingly subtle states of awareness (Gunaratana 1988; Sayadaw 2008; Shankman 2008).

Our prior brain mapping investigations of ACAM-J suggest that ACAM-J reorganizes the brain during meditation and may reveal insights into brain plasticity and mechanisms of attention, sensory processing, and cognitive control (Yang et al. 2024b). Recently, Yang et al. (2024a) demonstrated segregation of brain activity in the posterior and anterior aspects of the brain during ACAM-J, suggesting functional reorganization. Specifically, this prior study reported brain activity associated with ACAM-J in the precuneus, temporoparietal areas, and frontal regions, which are areas involved in attention, cognition, and perception. These findings indicate that investigating functional reorganization of ACAM-J can enhance our understanding of brain areas related to attention, cognition, and perception contributing to heightened states of consciousness (Taylor et al. 2013; Carhart et al. 2014; Girn et al. 2022).

Gradient analysis is a powerful method for quantitatively mapping functional reorganization of the brain in humans using functional magnetic resonance imaging (fMRI) (Margulies et al. 2016). Gradient analysis reduces complex and high-dimensional functional connectivity data into low-dimensional topographical representations called gradients, which allow for improved interpretability of brain organization and functional relationships between brain regions. Unlike traditional dimensionality reduction techniques, such as Principal Component Analysis, which focuses on capturing the maximum variance (Jolliffe 2002) or Independent Component Analysis, which assumes statistical independence of components (Hyvärinen and Oja 2000), gradient analysis employs a diffusion map embedding algorithm (Coifman and Lafon 2006). The diffusion map embedding algorithm captures continuous and hierarchical relationships between the functional connectivity of brain regions while simultaneously preserving local neighborhood relationships, or the similarity between nearby brain regions in terms of their connectivity patterns. Gradient analysis results in values at the extreme ends of the gradient space that represent continuous transitions that are not confined to discrete network boundaries (Margulies et al. 2016). Consequently, gradient analysis offers a unique advantage over traditional brain network analyses by capturing functional connectivity patterns in a continuous, low-dimensional space across the cortical surface that thereby enables interpretation of how functional relationships between brain regions are organized along continuous axes and how these spatial patterns relate to cognitive processes (Margulies et al. 2016).

Two consistent gradients that reflect meaningful features of cortical organization of the brain have emerged in prior studies (Margulies et al. 2016; Bernhardt et al. 2022; Girn et al. 2022). The first gradient, commonly referred to as the principal gradient, accounts for the most variance in connectivity and reflects the transition from unimodal sensorimotor regions to transmodal regions. Unimodal regions are those specialized in processing environmental stimuli like sound and vision, whereas transmodal regions are those that underlies higher cognitive functions and cross-modal information integration. Complementing the principal gradient, the secondary gradient represents the differences in functional organization between the visual cortex, the somatosensory cortex, and attention-related areas (Smith et al. 2006; Gazzaley et al. 2007; Margulies et al. 2016).

Gradient analysis has been applied in several clinical contexts (Park et al. 2022; Xia et al. 2022; Dong et al. 2023). More recently, its application has been extended to understanding functional brain reorganization related to psychedelics (Girn et al. 2022; Timmermann et al. 2023). For example, lysergic acid diethylamide and psilocybin have been shown to reduce the functional separation between the unimodal and transmodal cortices of the principal gradient (Girn et al. 2022). We hypothesize that ACAM-J may demonstrate similar gradient patterns to psychedelics due to several reasons. First, psychedelic experiences often include decreased self-referential thought and external awareness (Studerus et al. 2011; Preller et al. 2017); these subjective experiences are similar to those described in advanced meditation (Millière et al. 2018; Metzinger 2020; Yang et al. 2024b). Meditation is also associated with altered brain activity in brain areas related to self-referential thought and awareness (Hagerty et al. 2013; Taylor et al. 2013; Yang et al. 2024a) that are similar to those found in psychedelics (Millière et al. 2018; Girn et al. 2022). Thus, both advanced meditation and psychedelic states share similar qualitative characteristics and may thus share underlying patterns of brain activity (Venkatesh et al. 1997; Hagerty et al. 2013; Yang et al. 2024a).

In this context, we investigated cortical functional reorganization of the brain during ACAM-J using gradient analysis. We specifically addressed two questions: (i) Are the principal and secondary gradients altered during ACAM-J compared to non-meditative control conditions? And (ii) Are gradient alterations during ACAM-J associated with unique ACAM-J phenomenology? We hypothesized that gradient values of regions in the transmodal pole of the principal gradient will shift toward the middle of the principal gradient during ACAM-J. In contrast, we expect the opposite pattern for the secondary gradient: an increased separation between the visual network (VN) and the attention-related areas.

Materials and methods

This study reanalyzed data previously published (Yang et al. 2024a). The data collection and preprocessing methods, as described below, followed the same methodology as in the previous study. To meet the objectives of this study, the following analyses, as explained below, were performed differently from our previous study. The case-study methodology was established to collect high-quality data from a skilled meditator, which is extremely rare as achieving and maintaining ACAM-J states requires extensive training and practice, making it highly unlikely for meditation-naïve individuals to replicate them reliably. Therefore, our study was structured to enable intensive data collection from a skilled practitioner, with a focus on maximizing the reliability of findings. This approach was designed to minimize the risk of subject-specific effects and allow for validation of the individual effects observed in the subsequent group sample studies.

Participant

The subject of the case study was an adept meditator who was 52 yr old at the time of the data collection. The participant had an extensive background in ACAM-J with over 25 yr of

ACAM-J experience and a role as a long-term meditation teacher. His total training time amounts to a total of at least 20,000 h, which we calculated based on an estimated one to 2 h of daily practice from the start and approximately 1 yr of retreat with 14 h per day. The participant's meditation approach was more similar to sutta-jhana than the Visuddhimagga-jhana. The participant reported using formless objects such as consciousness and space as ACAM-J objects to enter the ACAM-J, and used the breath, bodily sensations, and width of concentration during the form jhanas (ACAM-J1 to ACAM-J4). The study was approved by the Mass General Brigham Institutional Review Board, and informed consent was signed by the participant.

Procedure

ACAM-J

fMRI data were collected over a period of 5 d, with each daily session lasting between 45 and 90 min, depending on the participant's comfort and fatigue levels. The participant was instructed to follow their routine ACAM-J practice (from ACAM-J1 to ACAM-J8) with their eyes closed. Each meditation session began with the participant achieving access concentration (AC), then progressing through ACAM-J1 to ACAM-J8.

To mark the transition from one state to the next, the participant pressed a button after each state, starting from AC. However, the participant did not indicate the transitions from ACAM-J6 to ACAM-J7 and from ACAM-J7 to ACAM-J8 as pressing the button would disrupt the natural progression to the next state for these ACAM-J states. As a result, the next button press occurred only after the participant had exited ACAM-J8, and these states were grouped together as ACAM-J6–8. We recorded 27 individual runs for each ACAM-J up to ACAM-J6, for a total of 162 runs (27 runs for each of the ACAM-J1–ACAM-J5, and 27 runs for ACAM-J6–8). The average time taken for a complete run, from ACAM-J1 to ACAM-J6–8, was approximately 512.01 s.

Non-meditative control conditions

We formulated two control conditions designed to engage the participant in non-meditative cognitive activities to contrast with the ACAM-J states. This selection was based on the phenomenology of the ACAM-J. We ensured that the control tasks were engaging enough to prevent the participant from involuntarily going into advanced meditative states. For this reason, we decided against using a resting-state control condition due to the likelihood of experienced meditators transitioning into meditative states (Cahn et al. 2010). Furthermore, these control conditions ensured consistency and reliability across runs, with the participant keeping their eyes closed during all tasks to match the meditation condition.

The first was the counting control condition, in which the participant was asked to mentally count down from 10,000 in increments of 5 for 8 min without moving their lips. The second was the memory control condition, in which the participant was asked to mentally revisit and narrate the events that occurred in the past 2 wk for 8 min, keeping their lips still for the duration of the task. Two iterations of each control task were performed, resulting in 16 min of data for each task. The initial iteration of these control tasks was collected prior to meditation runs. The subsequent iteration was performed on the fourth day of the fMRI data acquisition.

Note that our case study participant reported unintentionally entering meditative states during the first run of both of our control conditions, although with lesser intensity than in meditation itself. Specifically, in the memory condition, the frequency was 4/10 and intensity was 2/10, while in the counting condition, the frequency was 7/10 and intensity was 6/10. Excluding these runs did not affect the results (see Figs. S1 and S2), thus they were included in subsequent analyses (Yang et al. 2024a).

Neurophenomenology

In this study, we adopted a "neurophenomenological" methodology, which combines first-person experiential accounts of meditation with neuroimaging data to provide a more complete understanding of the meditative states (Sparby and Sacchet 2022). In total, we focused on seven phenomenological items. The first three items—"stability of attention" (level of calmness and tranquility, rated from poor to excellent), "width of attention" (the scope of attention, ranging from a narrow, laser-like focus to a broad, and fish-eye lens perspective), and "intensity" (the depth of the ACAM-J experience). The participant was asked to rate each phenomenological item based on their experience, and each item was scored on a scale from 1 to 10, with a higher score indicating a more intense manifestation of that item. The intensity, stability and width of attention were evaluated for each ACAM-J in each run, with a total of 27 runs for each of the ACAM-J states (ACAM-J1–J5 and ACAM-J6–8). Moreover, we examined the sensations in the body, which we categorized into four distinct types: "narrative thought stream," relating to the narrative thought contents arising during ACAM-J; "physical sensations," involving bodily sensations; "sights," referring to visual phenomena; and "sounds," referring to auditory experiences during ACAM-J. These sensations were rated collectively for the early stages of ACAM-J (ACAM-J1 to J4) and the later stages (ACAM-J5 to J8), on a scale ranging from 0 (not at all present) to 10 (extremely present).

Neuroimaging data acquisition

Brain imaging scans were conducted using a 7T MR scanner (SIEMENS MAGNETOM Terra) equipped with a 32-channel head coil. The functional imaging process was carried out using a single-shot 2D echo planar imaging sequence with T2∗-weighted BOLD-sensitive MRI. The parameters were as follows: repetition time (TR) was set at 2.9 s, echo time (TE) at 30 ms, flip angle (FA) at 75°, field of view (FOV) at [189 × 255], matrix at [172 × 232], GRAPPA factor at 3, and voxel size at $1.1 \times 1.1 \times 1.1$ mm^3, with 126 slices and an interslice distance of 0 mm. The entire brain was captured through sagittal oriented-interleaved slices, with phase encoding from anterior to posterior. Slices with opposite phase encoding (ie posterior-to-anterior) were also acquired to facilitate distortion correction.

Structural images of the whole brain were obtained using T1-weighted parameters: TR was set at 2.53 s, TE at 1.65 ms, inversion time at 1.1 s, FA at 7°, 0.8 mm isotropic resolution, FOV at 240 × 240, GRAPPA factor at 2, and bandwidth at 1,200 Hz/Px. Throughout the scanning session, the participant's physiological signals, including heart rate (measured by pulse oximetry) and respiration (measured by breathing bellows), were continuously recorded. However, these physiological signals were not further analyzed in this paper due to the study's primary focus on neuroimaging data and brain connectivity patterns. Our aim was to delve deep into these connectivity patterns and how ACAM-J alters the functional hierarchy in the brain through gradient analysis, and we intentionally chose not to distract from these objectives by integrating multiple dimensions of analysis within the same study. As a future direction, incorporating physiological measures could provide valuable insights into understanding how the changes observed within the body relate to ACAM-J.

Neuroimaging data Preprocessing

The fMRI data were subjected to a series of preprocessing steps, which were applied to each fMRI session and all runs within that session, similar to our previous study by Yang and colleagues (Yang et al. 2024a). The preprocessing steps included the following: (i) de-spiking, (ii) retrospective image correction, (iii) slice time correction, (iv) distortion correction, (v) motion correction, (vi) co-registration of anatomical dataset (T1) was registered to a standard MNI template, (vii) scrubbing, and (viii) nuisance regression and band-pass filtering (0.01–0.1 Hz).

Each fMRI run was then partitioned into distinct runs corresponding to different ACAM-J states (27 runs for each state). Moreover, each control run was further divided into one-minute segments to ensure comparability with the 2-min runs of each ACAM-J. This division resulted in 16 segments per control condition, ensuring comparability with the ACAM-J runs. Using shorter segments for control conditions also ensured reliable calculation of subsequent analysis, which would not have been feasible with 2-min segments due to the limited number of control runs. Finally, (ix) all fMRI data were smoothed with surface-smoothing of 6 mm FWHM.

Gradient analysis

First, Schaefer's 400-parcel atlas was used to create the cortical region-of-interest (ROI) parcellation. For each fMRI run, a 400×400 functional connectivity matrix was computed using Pearson's correlation, representing the functional connectivity between each pair of the 400 parcels. A mean correlation matrix was then computed from all these connectivity matrices to serve as the "reference template." This mean correlation matrix was then thresholded row-wise at 90% sparsity to retain only the strongest connections (Margulies et al. 2016).

To compute gradients, a similarity matrix was generated by calculating the cosine similarity to capture the similarity between connectivity patterns of ROIs. This similarity matrix served as the input to the diffusion map embedding algorithm (Coifman and Lafon 2006), which is a nonlinear dimensionality reduction technique used in gradient computation. Unlike other dimensionality reduction techniques, the diffusion map embedding algorithm preserves the local structure of data by modeling connectivity relationships as a diffusion process. It achieves this by computing eigenvectors of the similarity matrix, which represent the low-dimensional gradient space. The resulting gradients reflect smooth and continuous transitions in functional connectivity across the cortical surface (Margulies et al. 2016).

We extracted the first two gradients for subsequent analyses because they accounted for the greatest proportion of variance across the data (see results section for more details); the first two gradients often encapsulate the most salient dimensions of functional connectivity variations across the cerebral cortex (Margulies et al. 2016; Bernhardt et al. 2022). To facilitate comparison across our data segments, individual gradients were calculated and then aligned to the reference gradient template using Procrustes rotation with 10 iterations.

In gradient analysis, gradient values for each ROI are interpreted relative to their starting positions along the gradient and the networks they belong to. Unimodal networks, such as the somatosensory-motor network (SMN) and VN, are typically located at the extreme negative end of the principal gradient, while transmodal networks, such as the default mode network (DMN), are positioned at the extreme positive end. The proximity of gradient values reflects greater similarity in connectivity patterns, whereas greater distance indicates increased functional differentiation of connectivity patterns between networks (Margulies et al. 2016; Bernhardt et al. 2022).

A positive or a negative change in gradient values can have different implications depending on the ROI's initial position. For example, a positive change in the gradient value of an ROI within the DMN, which is already situated at the positive end of the gradient, indicates that it is becoming even more positive, increasing the gradient span at the transmodal end. Conversely, a positive change in the gradient value of an ROI within the VN, located at the negative end, indicates it is moving closer to the center of the gradient, reducing the span of the gradient at the unimodal end. Therefore, referring to unimodal networks at the negative end and transmodal networks at the positive end provides a consistent framework for interpreting these changes (Margulies et al. 2016; Smallwood et al. 2021; Girn et al. 2022). Finally, it is important to note that the assignment of positive and negative gradient values is arbitrary and used solely for comparative purposes.

Gradient analysis was performed using the BrainSpace toolbox in Python (Vos De Wael et al. 2020). By following closely with the established conventions, we ensured the validity of our findings (Wagstyl et al. 2015; Raut et al. 2020; Girn et al. 2022; Dong et al. 2023).

Statistical analysis

Gradient trends across ACAM-J

The trends' analysis was designed to investigate the cortical reorganization of the brain as the meditator progressed through ACAM-J, similar to the analysis used in our previous study (Yang et al. 2024a). We conducted linear mixed effect analysis for each of the 400 ROIs using the *lmer* package in R. These models included linear, quadratic, and cubic terms of ACAM-J as fixed effects, with individual ACAM-J segments treated as random effects. For optimal data representation, model complexity was adjusted based on the significance of higher-order terms. Following the approach of Yang et al., any non-significant highest-order term was removed from the model iteratively (Yang et al. 2024a). Finally, we applied a false discovery rate (FDR) correction to control for Type I errors, set at $p_{FDR} < 0.05$.

Comparisons between ACAM-J and control conditions

Our comparative analysis for ACAM-J and the control conditions comprised of two levels which, were identically repeated for both the principal and the secondary gradients: (i) network-level and (ii) ROI-level analyses. For network-level analysis, we first computed the mean gradient values for each of the Yeo's 7 networks, namely, SMN, VN, dorsal attention network (DAN), salience network (SN), frontoparietal control network (CN), limbic network (LN), and DMN (Yeo et al. 2011; Schaefer et al. 2018). Then, we compared mean gradient values of each network from ACAM-J1 to ACAM-J6–8 with the control conditions. For the ROI-level analysis, pairwise comparisons of the gradient values across 400 ROIs between the control conditions and ACAM-J states were conducted to gain greater spatial resolution of gradient changes in ACAM-J. For both analyses, we implemented mixed-effects linear models using the *lmer* package in R. We set the control conditions (ie counting or memory) as the reference group, against which each ACAM-J was compared to as fixed effects. Each individual run was treated as a random effect, allowing us to account for the non-independence of observations within each run. FDR correction at $p_{FDR} < 0.05$ was applied to control for the rate of Type I errors due to multiple network and ROI comparisons.

First two gradients and ACAM-J phenomenology

To investigate the relationship between gradients and ACAM-J phenomenology, we used both correlation and multiple linear regression analyses. The choice of these statistical methods was guided by the structure of the data, the goals of the analysis, and the sequential nature of ACAM-J.

Specifically, correlation analysis was applied to examine the relationship between the gradient values and the intensity of ACAM-J, stability of attention, and width of attention. Correlation was chosen because our aim was to assess direct associations between gradient values and phenomenological ratings. Unlike regression, correlation captures one-to-one relationships between variables (Schober et al. 2018), eliminating the need to partition the effects of individual ACAM-J states on these attributes. Importantly, treating individual ACAM-J states as separate predictors in a regression model for these attributes would imply that variance in earlier states (eg ACAM-J1) could be accounted for by later states (eg ACAM-J2 to ACAM-J5). Such an assumption would contradict the progression-based nature of ACAM-J, where later states are inherently dependent on the earlier states. Instead, correlation analysis allowed us to directly examine how gradient values correspond to variations in intensity, stability, and width of attention, which were consistently rated for each ACAM-J state (ACAM-J1 to ACAM-J8) and for each run.

On the other hand, for the other phenomenology category—which includes narrative thought stream, physical sensations, sights, and sounds—we conducted multiple linear regression analysis. The structure of our data dictated this choice: while the first three phenomenological attributes were evaluated on both a per-ACAM-J and per-run basis, the other four ratings combined early (ACAM-J1–4) and late (ACAM-J5–8) ACAM-J states, resulting in two observations per run for each category. Multiple regression allowed us to model the contributions of individual ACAM-J states (eg ACAM-J1 and ACAM-J2) to these aggregated early and late ratings, providing insight into how each ACAM-J influenced the grouped phenomenological ratings. Correlation analysis would not have been suitable to capture the contributions of multiple predictors to these grouped ratings. We acknowledge that the limited number of observations (two per run for each aggregated category) poses challenges. However, given the primary aim of decomposing how individual ACAM-J states contribute to the aggregated ratings, multiple regression was chosen as the most appropriate method.

The analysis proceeded in two steps. Our first step involved correlation analysis, where we correlated the gradient values of each of the 400 ROIs with our target phenomenological ratings (namely, "width of attention," "stability of attention," and "intensity of ACAM-J") using Pearson's correlation coefficient. Following this, we utilized multiple linear regression analysis with the remaining early and late phenomenological categories as the predicted outcome, using gradient values for each ROI as a predictor across different ACAM-J states (from ACAM-J1 to ACAM-J8). Given the interconnected nature of gradient values and the relative positioning of ROIs within a continuous connectivity space, applying standard multiple comparison corrections such as FDR—which assume independent tests—would have been overly conservative and potentially obscured meaningful relationships (Hong et al. 2020). Instead, we have reported uncorrected *P*-values, acknowledging its limitations. All these procedures were conducted for both the principal and secondary gradients.

Table 1. Proportion of variance accounted for each condition in the principal and secondary gradient.

	Principal gradient	Secondary gradient
ACAM-J1	39.52%	24.26%
ACAM-J2	36.01%	24.61%
ACAM-J3	38.12%	21.48%
ACAM-J4	35.17%	19.39%
ACAM-J5	35.86%	22.11%
ACAM-J6–8	37.78%	21.71%
Memory Control	38.88%	14.80%
Counting Control	49.79%	18.83%
Average	38.89%	20.90%

Results

Principal gradient

We observed varying proportions of variance across different ACAM-J states and control conditions (Table 1). On average, the principal gradient contributed to 39% of the variance. ACAM-J1 displayed the highest variance, approximately 40%, while ACAM-J4 displayed the lowest at about 35%. The variance for other ACAM-J states was within the following range: 36% for ACAM-J2, 38% for ACAM-J3, 36% for ACAM-J5, and 38% for ACAM-J6–8. In comparison, the control conditions displayed around 39% for memory control and 50% for counting control.

Furthermore, we have plotted the principal gradient mean values for each ACAM-J state (ACAM-J1 to ACAM-J6–8) together with the memory and counting control conditions to provide a clearer visualization of gradient patterns across conditions (Fig. 1).

ACAM-J trends

Linear mixed-effects model revealed significant linear, quadratic, and cubic trends across ACAM-J. Positive linear trends were observed in the regions of the CN, particularly in the lateral prefrontal cortex (PFCl) and parietal areas, whereas negative trends were observed in the DMN within precuneus and posterior cingulate cortex (PCC) (Fig. 2). Positive linear trends were also observed in the parietal operculum, and negative trends were observed in the temporal-occipital areas of the SN. Finally, positive linear trends were observed in the VN. We also identified a positive quadratic trend in the PFCl within the boundaries of CN. Moreover, cubic trends were identified in various regions across ACAM-J. More specifically, positive cubic trends were identified within regions of the CN, particularly the PFCl and parietal areas, PFC and parietal regions of the DMN, and in the parietal operculum area of the SN (Fig. 2). In contrast, we found negative cubic trends in the DAN, covering the postcentral area, and in the VN.

Comparisons with non-meditative control conditions

The network-level principal gradient value comparisons revealed several significant differences between the control conditions and ACAM-J (Fig. 3). For DAN, all ACAM-J except ACAM-J1 had higher principal gradient values than the counting control condition. Similarly, for CN, ACAM-J3, ACAM-J5, and ACAM-J6–8 had higher principal gradient values than the memory control condition. In contrast, for DMN, all ACAM-J had lower principal gradient values than the counting control condition. These results suggest significant variations in mean principal gradient values across ACAM-J in comparison to the control conditions, indicating changes in functional reorganization of DAN, CN, and DMN across ACAM-J.

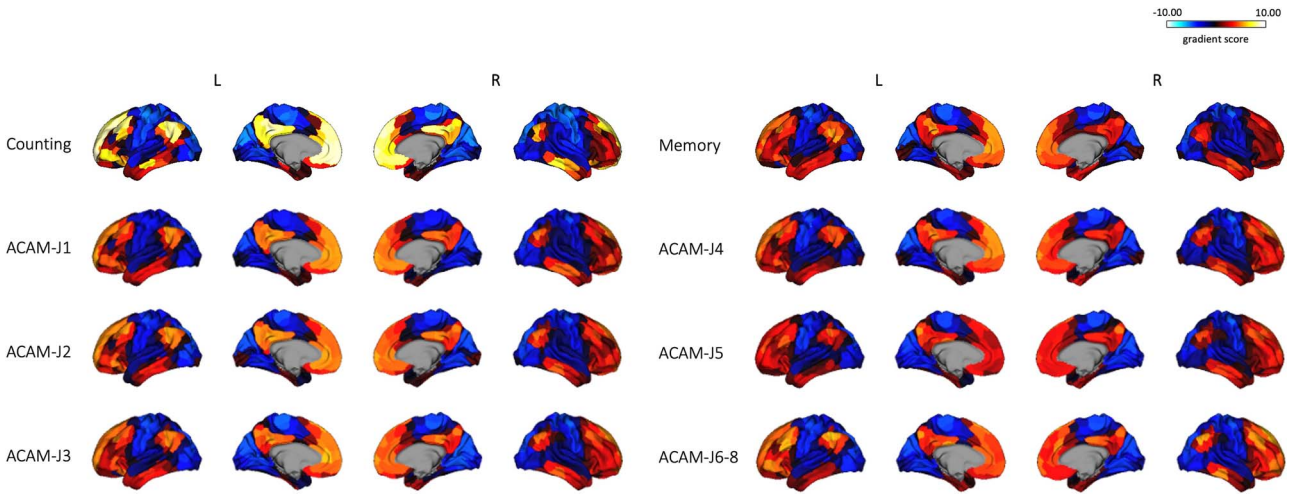

Fig. 1. Mean principal gradient values across ACAM-J states and control conditions. Visualization of the mean principal gradient values for each ACAM-J state (ACAM-J1 to ACAM-J6–8) alongside the memory and counting control conditions.

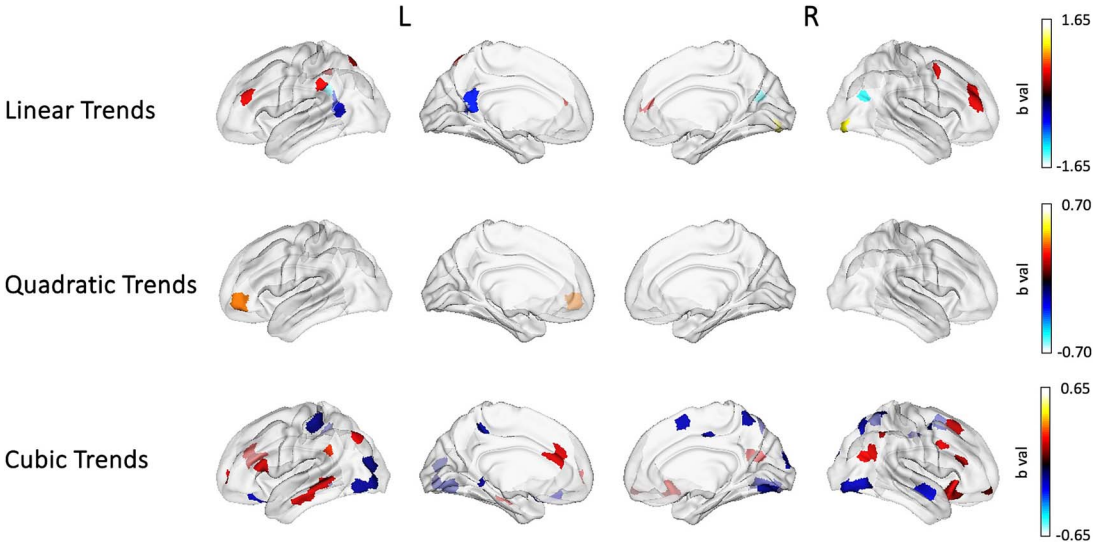

Fig. 2. Significant linear, quadratic, and cubic ACAM-J trends for principal gradient. Visualization of trends across ACAM-J states separated into linear, quadratic and cubic trends for the principal gradient at $p_{FDR} < 0.05$.

The ROI-level analysis revealed that ACAM-J, compared to the counting control condition, consistently showed increased principal gradient values for the CN (parietal and PFCl) regions. This increase became more pronounced from ACAM-J1 to ACAM-J6–8 (Fig. 3). On the other hand, some regions in CN, especially the precuneus showed negative principal gradient values compared to the counting control. Moreover, ACAM-J became less positive compared to counting control with decreasing principal gradient values in DMN (parietal, precuneus, PCC, dorsal, and medial PFC; PFCm). Regions in the DAN (postcentral gyrus, frontal eye fields) showed an increase in principal gradient values throughout ACAM-J when compared to the counting control. The areas in SN (medial, temporal, parietal, frontal operculum, and insula) also exhibited increased principal gradient values, whereas occipital areas exhibited decreased principal gradient values compared to the counting control. The areas within SMN showed a gradual increase in principal gradient values, while the ones in VN demonstrated a pattern with an increase in principal gradient values that peaked at ACAM-J4, followed by a gradual decrease as ACAM-J deepened toward ACAM-J6–8.

As ACAM-J deepened, the difference between ACAM-J and the memory control condition became larger: regions within CN (cingulate cortex and PFCl) showed increasing principal gradient values and regions within the precuneus showed principal gradient values (Fig. 3). Throughout ACAM-J, areas within the DMN particularly in the precuneus and PCC, showed decreased principal gradient values compared to the memory control condition, similar to those observed in comparison to counting control. ACAM-J exhibited decreased principal gradient values in the postcentral region of the DAN and the temporal and occipital regions of the SN. Finally, across all ACAM-J, VN displayed a decrease in principal gradient values compared to the memory condition which contrasted with the counting control.

Neurophenomenology

For width of attention, principal gradient values in regions of the CN (PFCl and parietal areas), DAN (postcentral) and SN (insula, parietal, and frontal operculum) exhibited positive correlations with width of attention (Fig. 4), while principal gradient values in regions within the SMN and DMN (precuneus and PCC)

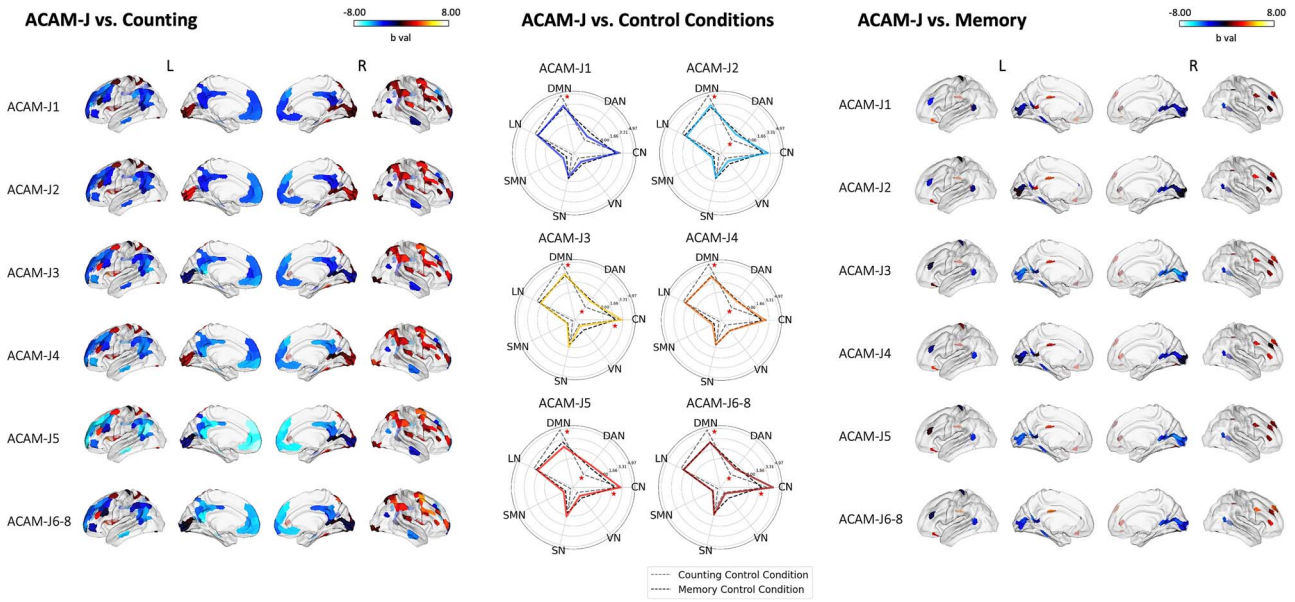

Fig. 3. Statistical results for the principal gradient. The left section of the plot shows the significant principal gradient values of ACAM-J compared to the counting control condition. The right section of the plot shows the significant principal gradient values of ACAM-J compared to the memory control condition. Finally, the middle plot shows spider plots for the mean network principal gradient values of ACAM-J compared to the counting and memory control conditions. Red asterisk marks on the control condition in the spider plot demonstrate significant mean network gradient differences between a particular ACAM-J and the control condition. $* p_{FDR} < 0.05$. DMN = default mode network, DAN = dorsal attention network, CN = frontoparietal control network, VN = visual network, SN = salience network, SMN = somatosensory-motor network, LN = limbic network.

exhibited negative correlations. For stability of attention, principal gradient values in regions of the SN (insula, medial subregion, and frontal operculum), SMN, and VN, demonstrated positive correlations, while regions in the CN (precuneus), DMN (precuneus and PCC), and DAN (postcentral) showed negative correlations. Finally, for intensity of ACAM-J, principal gradient values in regions of SN (insula, temporal, occipital, parietal, medial subregions, and frontal operculum) and SMN exhibited positive correlations, whereas regions within the CN (precuneus), DMN (precuneus and PCC), and DAN (postcentral) displayed negative correlations.

The results of early neurophenomenology displayed a positive association between narrative thought stream ratings and DMN (precuneus and PCC) principal gradient values and a negative association with SMN and SN principal gradient values (Fig. 5) Late neurophenomenology results demonstrated a positive association between narrative thought stream ratings and DAN principal gradient values. Early sensation of sights displayed a positive association with gradient values within temporal areas of the LN, indicating that higher ratings of visual experiences corresponded with increased principal gradient values in these areas. For late sensation of sights, there was a negative association with principal gradient values within the SMN, suggesting that lower SMN principal gradient values are associated with more intense visual ratings. Higher early and late sensation of sounds were associated with higher principal gradient values within the posterior areas of the DAN. Finally, early sensation of sounds was associated with lower principal gradient values in the SMN.

Secondary gradient

For the secondary gradient, we observed various proportions of variance between the different ACAM-J states and control conditions (Table 1). The average variance accounted by the secondary gradient was 21%. ACAM-J1 and ACAM-J2 displayed the highest variances, approximately 24% each, while ACAM-J4 displayed the lowest, at around 19%. The variance for other ACAM-J states also varied: ACAM-J3 at 21%, ACAM-J5 at 22%, and ACAM-J6–8 at 22%. For the control conditions, the variance was at approximately 15% for the memory control and at 19% for the counting control.

Additionally, we have visualized the mean values of the secondary gradient for each ACAM-J state (ACAM-J1 to ACAM-J6–8), alongside the memory and counting control conditions, for a clearer depiction of gradient patterns across the conditions (Fig. 6).

ACAM-J trends

Positive linear trends were observed in the CN, particularly in the PFCl (Fig. 7). In contrast, mixed (positive and negative) linear trends were observed in the regions within the SMN. Furthermore, a negative linear trend was observed in VN. We also observed a negative quadratic trend in the SMN. For cubic trends, the results varied across regions. Positive cubic trends were identified in CN, involving the PFCl similar to the linear trends (Fig. 7). On the other hand, a mixed trend (positive and negative) was observed in DMN, specifically, including a positive trend of secondary gradient values in PFC and a negative trend of secondary gradient values in temporal areas. Negative cubic trends were also present in postcentral areas and frontal eye fields of the DAN, orbitofrontal cortex, and temporal pole of LN and in SMN. Finally, in VN, there was a mix of positive and negative cubic trends.

Comparisons against non-meditative control conditions

Our network-level analysis revealed significant differences between the memory control condition and the ACAM-J (Fig. 8). For SN, all ACAM-J displayed higher secondary gradient values than the memory control condition. Furthermore, ACAMJ-5 and ACAM-J6–8 had higher secondary gradient values for CN compared to the memory condition. On the other hand, all ACAM-J had lower secondary gradient values for VN relative to the memory control condition. Compared to the counting control, ACAM-J1 exhibited lower secondary gradient values in CN, while

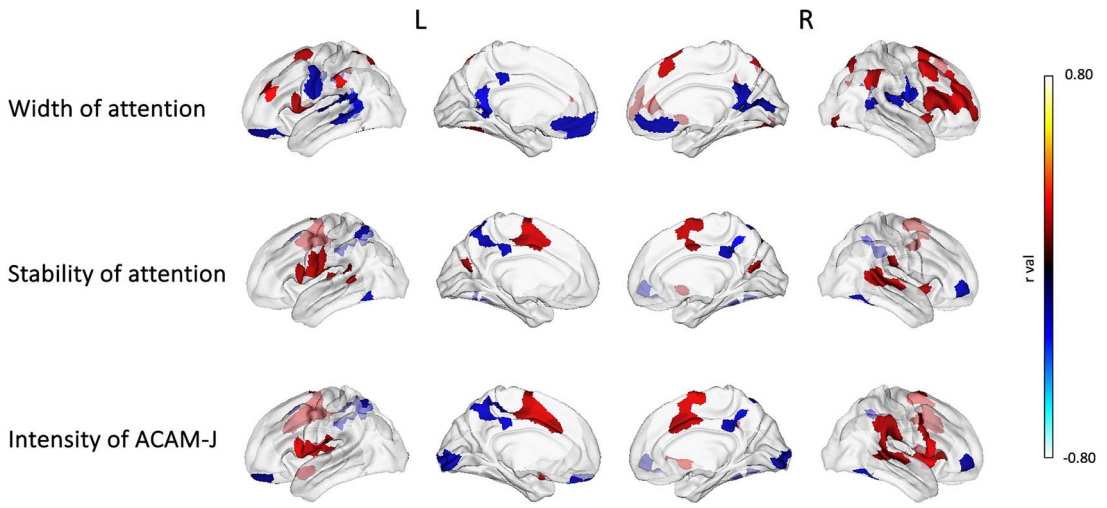

Fig. 4. Association between principal gradient values of ACAM-J and phenomenology. Visualization of the correlation between gradient values within the principal gradient and width of attention, stability of attention, and intensity phenomenology. Results were uncorrected for multiple comparisons due to the interdependence of ROI gradient values.

all ACAM-J except for ACAM-J5 showed lower secondary gradient values in DAN.

The ROI-level analysis for both counting and memory control conditions compared to ACAM-J revealed general similar secondary gradient trends within the brain, with a clear separation between the VN and SN (Fig. 8).

For the counting control, ACAM-J showed greater positive secondary gradient values in CN in PFCl and cingulate cortex and negative secondary gradient values in parietal areas. Regions in the DMN showed a mix of positive and negative secondary gradient values for ACAM-J when compared to the counting control, with precuneus, PCC, and ventral PFC (PFCv) displaying positive secondary gradient values whereas temporal and PFC displaying negative secondary gradient values. As ACAM-J progressed, areas within the DAN (postcentral gyrus) showed negative secondary gradient values compared to the counting condition. Furthermore, negative secondary gradient values were observed in temporal areas of LN and positive secondary gradient values were observed in orbitofrontal cortex regions in LN for ACAM-J. In contrast, the SN (frontal operculum and insula, medial and parietal operculum, temporal, occipital, and parietal) displayed positive secondary gradient values for ACAM-J compared to counting control. This positive change in gradient values toward the positive extreme end of the secondary gradient was consistent and strong throughout all the ACAM-J states. The SMN exhibited a mix of positive and negative secondary gradient values compared to the counting control. Finally, VN areas were negative across all ACAM-J compared to counting control, becoming more extreme on the negative end of the secondary gradient, with the intensity of these negative secondary gradient values remaining stable but strong throughout the ACAM-J.

Compared to the memory condition, ACAM-J consistently showed positive secondary gradient values in CN areas (PFCl, PFCv, and cingulate cortex). The DMN areas displayed mixed (positive and negative) secondary gradient values, like the comparisons with counting conditions, with positive secondary gradient values in precuneus, PCC, and PFCv and negative secondary gradient values within temporal areas and the PFC. For DAN, postcentral areas were also mixed, displaying positive and negative secondary gradient values, whereas frontal eye field regions exhibited positive secondary gradient values. The regions within SN (frontal operculum and insula, medial and parietal operculum, temporal, occipital, and parietal) exhibited positive secondary gradient values across all ACAM-J compared to the memory condition, like the counting condition. SMN areas demonstrated a mix of positive and negative secondary gradient values. Finally, the areas within VN showed strong negative secondary gradient values, like the counting condition, highlighting a contrast in functional organization of visual processing areas with salience/attention areas across all ACAM-J.

Neurophenomenology

Higher width of attention was positively correlated with secondary gradient values in regions of the CN (PFCl and parietal regions), DMN (precuneus and PCC), and negatively associated with secondary gradient values of areas in SMN, temporal regions within DMN, and LN (Fig. 9). In contrast, secondary gradient values for regions within DAN, SN, and VN showed a mix of positive and negative correlations with width of attention. Stability of attention demonstrated positive correlations with secondary gradient values in regions of the CN (PFCl and parietal areas), DMN (PFCv) and SN (frontal operculum and insula), and negative correlations with secondary gradient values in regions of the DAN (postcentral), SMN, and VN. For the intensity of ACAM-J qualities, positive correlations were observed within secondary gradient values in regions of the CN (PFCl and parietal regions), DMN (precuneus, PCC, and PFCv), and SN. While negative correlations were observed with secondary gradient values of regions within SMN and VN.

For the early neurophenomenology we observed a positive association between early narrative thought stream ratings and the secondary gradient values of areas within SMN and posterior regions of DAN. Furthermore, there was a negative association between early narrative thought stream ratings and secondary gradient values of the temporal areas within the DMN (Fig. 10). For late neurophenomenology, we observed that higher narrative thought stream ratings correspond with higher secondary gradient values in the PFC of the DMN. Early and late physical sensations exhibited variable results, showing both positive and negative associations across secondary gradient values of PFC within DMN throughout the ACAM-J states. Early and late sensation of sights showed a negative association with secondary

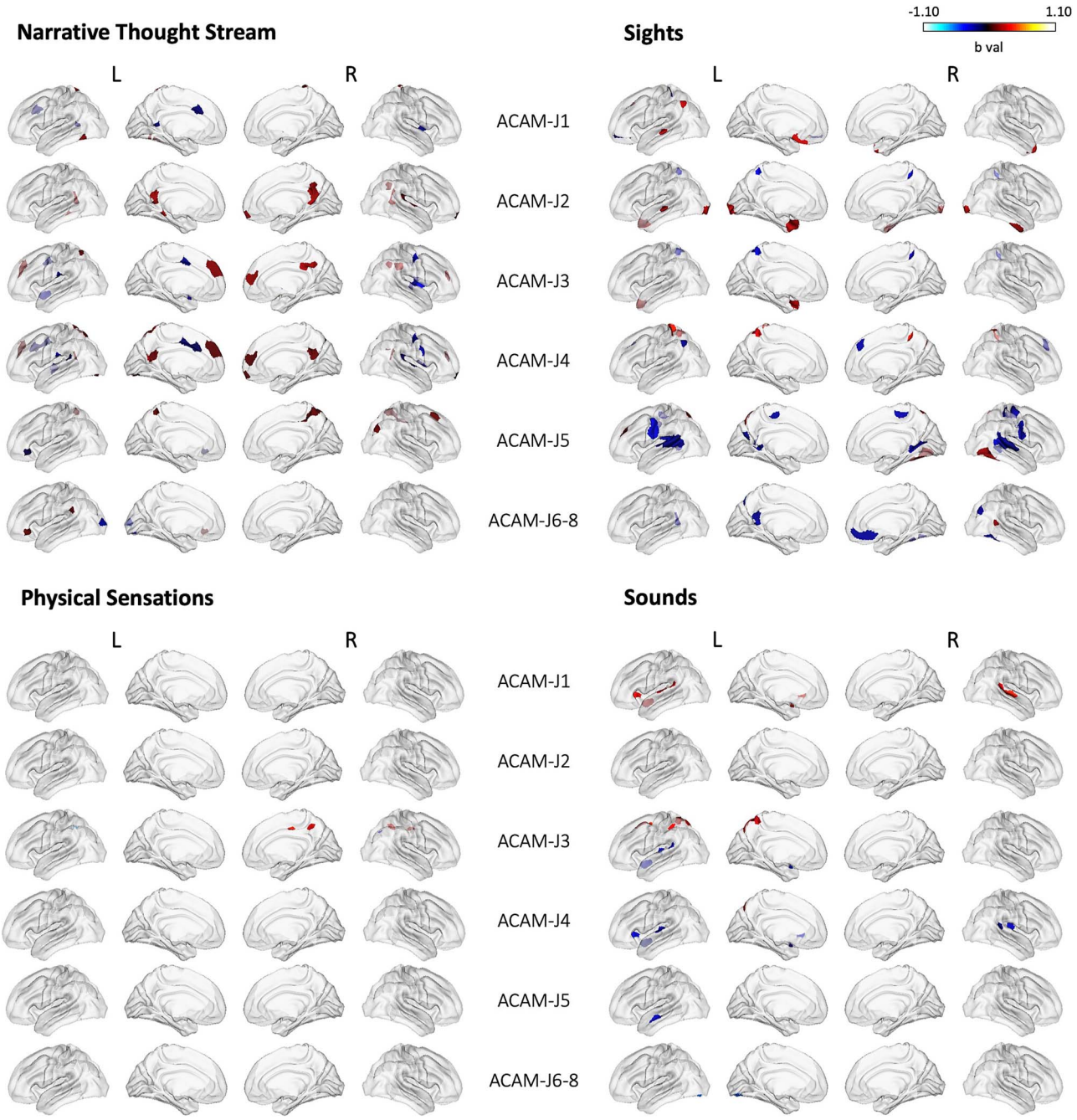

Fig. 5. Association between principal gradient values of ACAM-J and early and late sensations. This figure visualizes significant principal gradient results as the predictor of sensations phenomenology ratings which include narrative thought stream, physical sensations, sights and sounds. Early sensations range from ACAM-J1 to ACAM-J4 and late sensations range from ACAM-J5 to ACAM-J6–8. Results were uncorrected for multiple comparisons due to the interdependence of ROI gradient values.

gradient values in SMN. Furthermore, late sensation of sights had a positive association with secondary gradient values in the posterior and frontal eye fields of DAN, indicating that higher ratings of sights are linked to increased secondary gradient values in these areas. For sensation of sounds, we observed that higher ratings were associated with variable secondary gradient values in the SMN, with the first ACAM-J states (ACAM-J1 to ACAM-J4) displaying a positive association and the late ACAM-J states (ACAM-J5 to ACAM-J8) displaying a negative association. Finally, we observed positive associations between the late sensation of sounds ratings and the secondary gradient values of the temporal areas in the DMN and LN, indicating that higher ratings correspond with higher secondary gradient values.

Discussion

The current study implemented a nonlinear dimensionality reduction technique called gradient analysis to investigate brain reorganization during ACAM-J and combined it with a neurophenomenological approach to understand how this reorganization may relate to experience. Gradient analysis interprets high-dimensional data in less complex forms, revealing

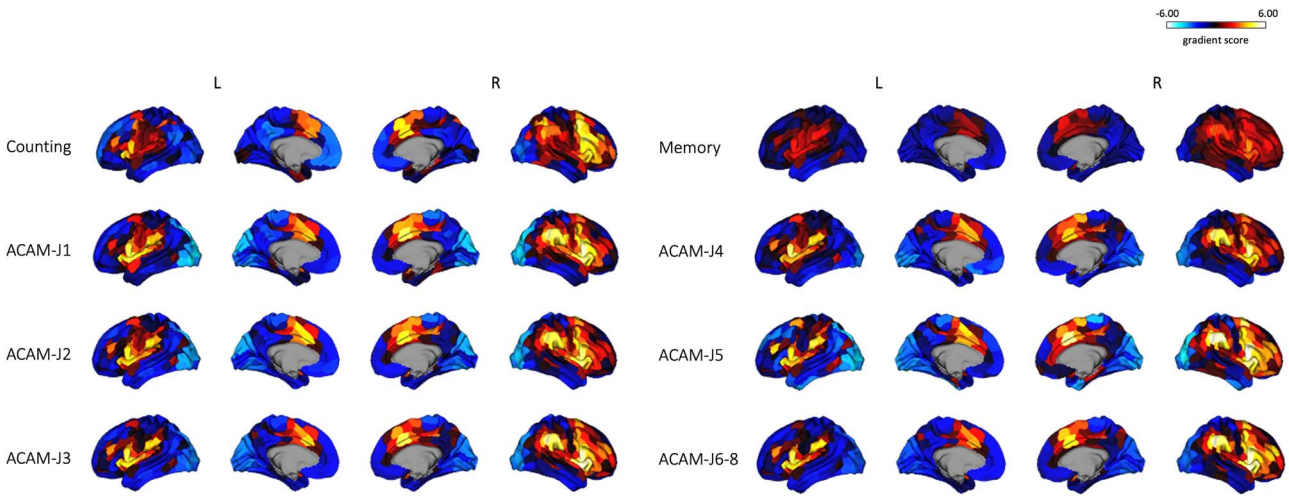

Fig. 6. Mean secondary gradient values across ACAM-J states and control conditions. Visualization of the mean secondary gradient values for each ACAM-J state (ACAM-J1 to ACAM-J6–8) alongside the memory and counting control conditions.

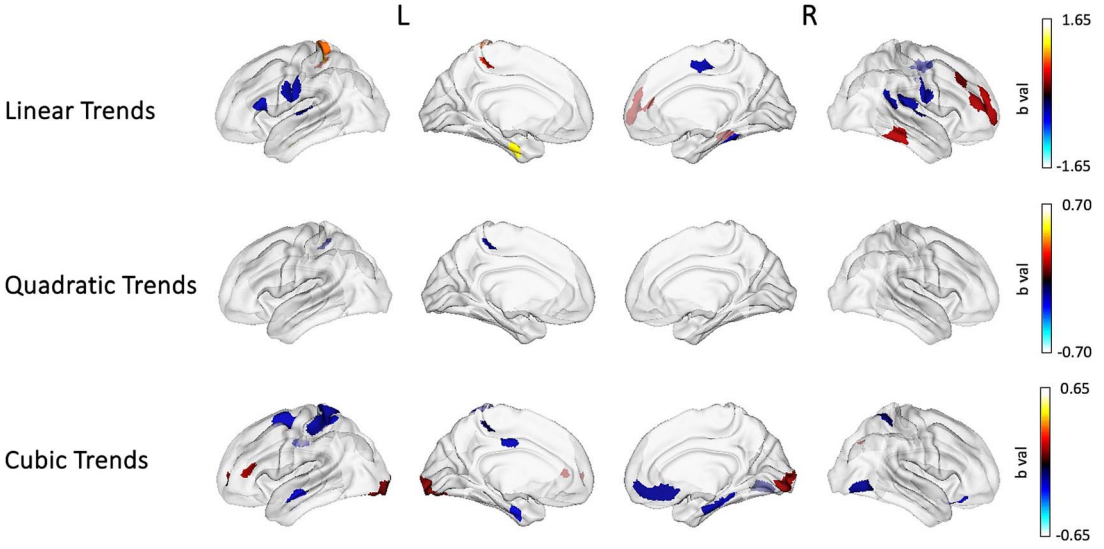

Fig. 7. Significant linear, quadratic, and cubic ACAM-J trends for secondary gradient. This figure visualizes trends across ACAM-J states separated into linear, quadratic, and cubic trends for the secondary gradient at $p_{FDR} < 0.05$.

a continuous spectrum of values in terms of connectivity patterns that represent the functional organization of the brain. Main findings from this study are: (i) ACAM-J flattens the principal gradient by decreasing gradient values within the DMN; (ii) expansion of the secondary gradient at the two extreme ends, displaying lower gradient values in VN and higher gradient values in attention-related SN areas. Overall, these results suggest functional reorganization of the brain during ACAM-J, including of brain areas related to attention and cognitive control, as well as sensory processing.

The principal gradient has been extensively studied and consistently replicated (Margulies et al. 2016; RAI et al. 2020; Bernhardt et al. 2022) and represents the functional hierarchy in the brain from low-level sensory processing to high-level and abstract cognitive processing (Wagstyl et al. 2015; RAI et al. 2020; Bernhardt et al. 2022; Xia et al. 2022). Our findings indicate that ACAM-J alters the principal gradient toward a globally integrated state. The most prominent finding was a negative shift in principal gradient values of the DMN across ACAM-J and compared to both control conditions. Gradient values at the positive extreme end of the principal gradient shifted toward a less extreme position, evident in both network-level and ROI-level analyses, particularly in the precuneus and PCC. Neurophenomenology results also revealed that negative gradient values within the precuneus and PCC, both important regions of the DMN and CN, were associated with higher stability of attention and intensity of ACAM-J and lower early sensations of the narrative thought stream. The precuneus, a core component of the DMN, plays an important role in executive function (Yeager et al. 2022). We previously found correlations between brain activity in the precuneus and attentional qualities during ACAM-J (Yang et al. 2024b). These observations support the idea that as the functional connectivity patterns in the brain become more globally integrated, moving away from the extreme transmodal end of the gradient, ACAM-J meditators may experience a decrease in narrative thoughts and an increase in present-centered awareness. However, given the lack of multiple comparison correction, these findings should be interpreted as preliminary and require further hypothesis-driven research.

We also observed changes at the unimodal end of the principal gradient, especially in the DAN (postcentral gyrus) and SN (insula, parietal, and frontal operculum). Compared to the

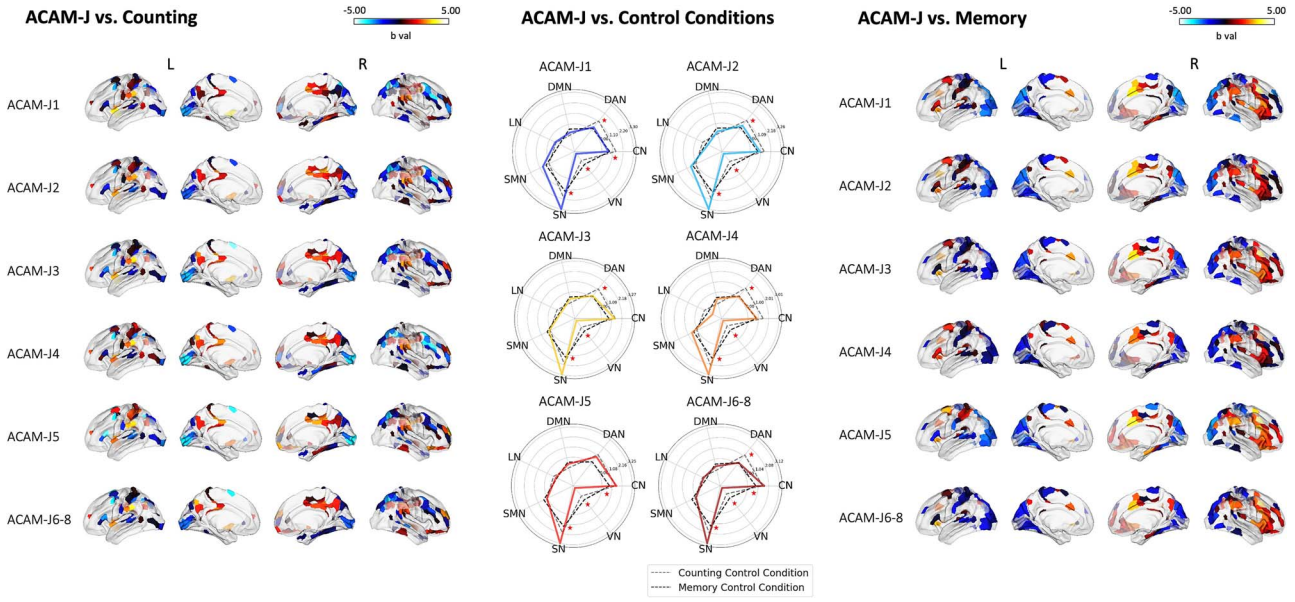

Fig. 8. Statistical results for the secondary gradient. The left section of the plot shows the significant secondary gradient values of ACAM-J compared to the counting control condition. The right section of the plot shows the significant secondary gradient values of ACAM-J compared to the memory control condition. Finally, the middle plot shows spider plots for the mean network secondary gradient values of ACAM-J compared to the counting and memory control conditions. Red asterisk marks on the control condition in the spider plot demonstrate significant mean network secondary gradient differences between a particular ACAM-J and the particular control condition. $* \ p_{FDR} < 0.05$. DMN = default mode network, DAN = dorsal attention network, CN = frontoparietal control network, VN = visual network, SN = salience network, SMN = somatosensory-motor network, LN = limbic network.

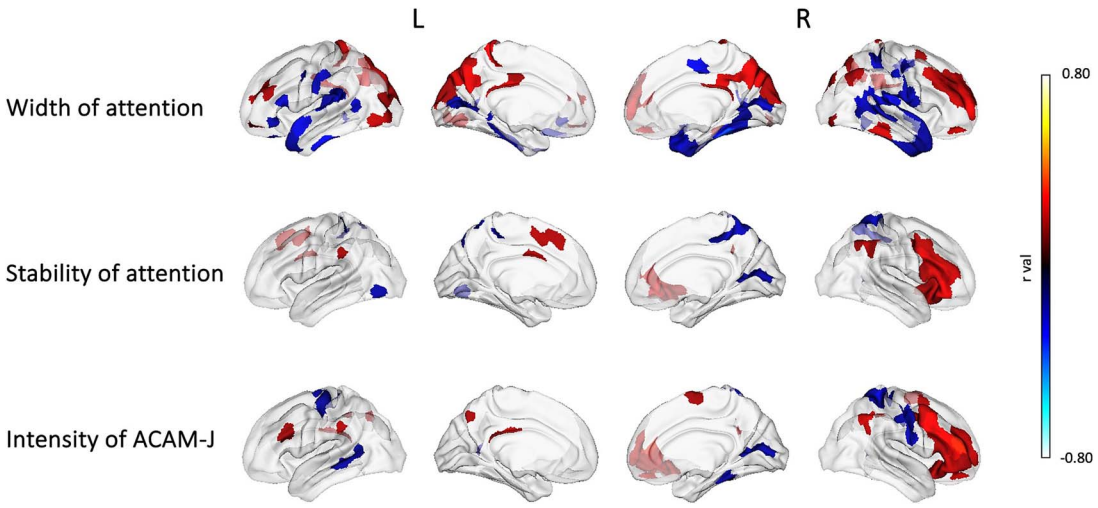

Fig. 9. Association between secondary gradient values of ACAM-J and phenomenology. This figure visualizes the correlation between gradient values within the secondary gradient and width of attention, stability of attention, and intensity phenomenology. Results were uncorrected for multiple comparisons due to the interdependence of ROI gradient values.

counting control condition, these regions showed a shift toward the middle of the principal gradient across both network-level and ROI-level analyses during ACAM-J. Compared to the memory control condition, ACAM-J displayed a positive shift from the unimodal end of the gradient toward the middle in principal gradient values in regions within the SMN. Furthermore, positive linear trends in principal gradient values were noted in regions within the SN and VN throughout ACAM-J. Regions within the DAN and SN are known to be integral for attentional control and sensory integration (Fox et al. 2006; Uddin 2015). The observed changes at the unimodal end of the principal gradient may support the rapid interoceptive information processing and flexible attention during ACAM-J, given that the SN, particularly the insula, is associated with sensitivity to salient events (Menon and Uddin 2010; Centanni et al. 2021). These findings suggest a de-emphasis on sensorimotor processes during ACAM-J, aligning with the meditative process of detaching from external sensory stimuli and redirecting attention internally (Brasington 2015). We observed that the neurophenomenological analysis also revealed positive correlations between principal gradient values in the DAN (postcentral) and SN (insula, parietal, and frontal operculum) with width of attention.

While the overall findings were consistent across both control conditions, it is important to address an inconsistency in the ROI-level analysis results for the principal gradient. The changes for ACAM-J relative to the counting condition were as expected,

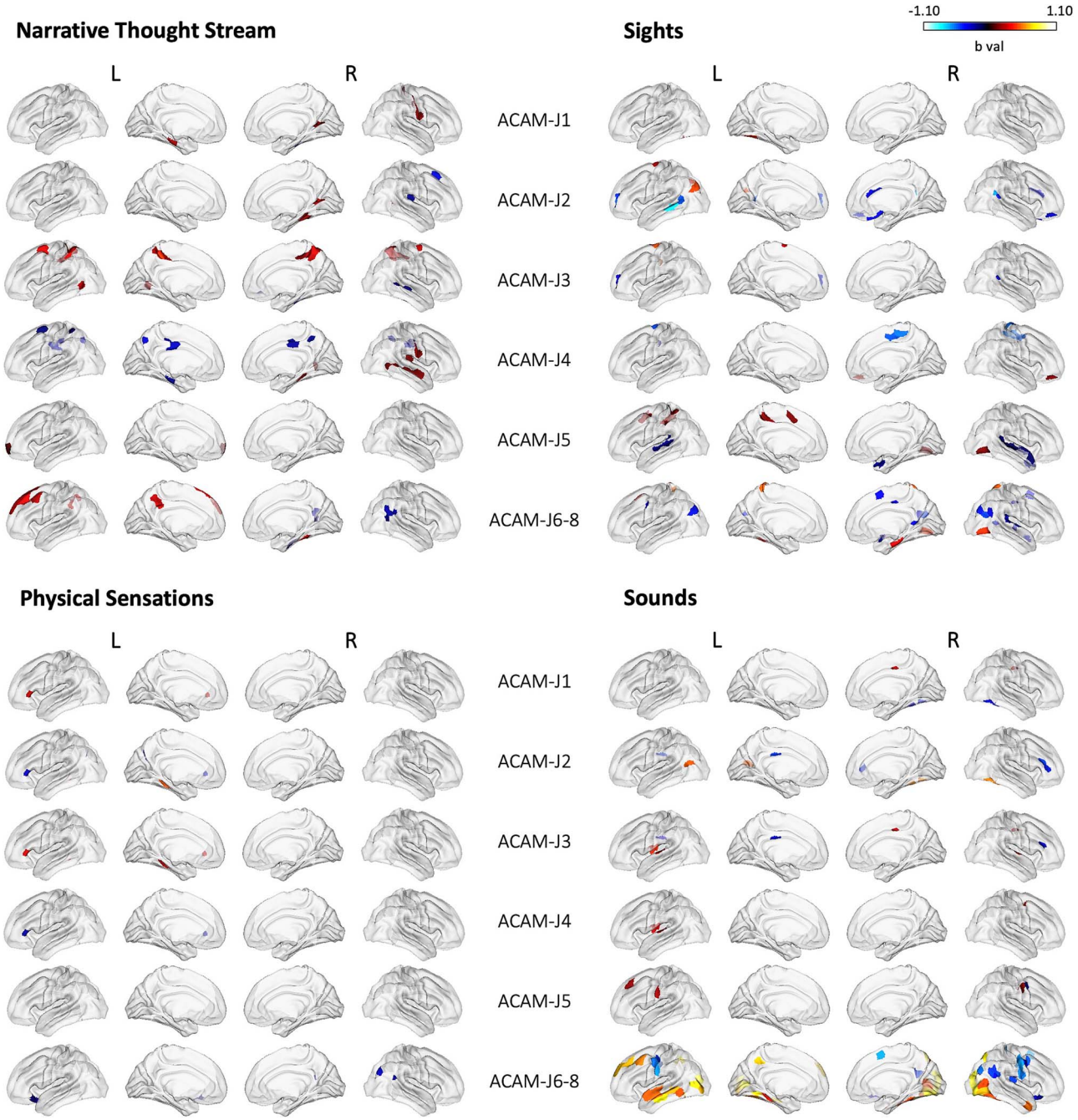

Fig. 10. Association between secondary gradient values of ACAM-J and early and late sensations. Visualization of significant gradient results as the predictor of sensations phenomenology ratings which include narrative thought stream, physical sensations, sights and sounds. Early sensations range from ACAM-J1 to ACAM-J4 and late sensations range from ACAM-J5 to ACAM-J6–8. Results were uncorrected for multiple comparisons due to the interdependence of ROI gradient values.

with a positive shift from the unimodal end of the principal gradient toward the middle and involved networks such as SN, DAN, SMN, and VN. However, this pattern was not replicated in the ROI analysis when comparing ACAM-J with the memory control condition. This difference might be attributed to the unique influence that memory recall has on the principal gradient. One plausible explanation can be that the memory condition also affects these lower-order sensory processing areas (Favila et al. 2022); particularly, memory recall involving vivid, sensory-rich content might activate these primary sensory and motor areas. As a result, the memory condition may inadvertently cause changes in the unimodal end of the gradient. This effect overlap for lower-order sensory areas may explain the absence of a significant difference in principal gradient values for these regions between the ACAM-J and memory condition. Both conditions might lead to a similar functional organization, but through different mechanisms: ACAM-J through a meditation-induced blurring of sensory and cognitive processing, and memory recall through the activation of sensory and motor areas associated with the revisited experiences. In addition to this, the SN, which plays a key role in directing attention, might be similarly modulated in both conditions. In ACAM-J, this network might facilitate the integration of sensory and cognitive processes, while in memory recall, it may facilitate navigation between memories and the external sensory environment (Christopher et al. 2015). Therefore, the absence of significant differences between the ACAM-J and memory

conditions might be attributed to the similar influence of lower-order sensory networks on the principal gradient, although through different cognitive processes.

Despite these similarities, we chose to include both counting and memory conditions in the study to highlight the distinct mechanisms and contrasts they offer when compared to ACAM-J. This approach provides a more robust understanding of hierarchical organization of the brain across both gradients during ACAM-J.

The secondary gradient is characterized by the dissociation of the VN from areas related to sensory/motor functions and attention (Zhang et al. 2019; RAI et al. 2020; Jiang et al. 2023). However, it is important to note that there are some variations in functional organization reported within the secondary gradient in previous studies (Zhang et al. 2019; RAI et al. 2020; Jiang et al. 2023). Our findings reveal an expansion of the secondary gradient during ACAM-J. Specifically, we found that secondary gradient values in the VN became more negative compared to both control conditions, while SN demonstrated greater positive gradient values. Trends analyses further revealed decreasing secondary gradient values in the VN and increasing secondary gradient values in the SN across ACAM-J. These results are particularly important in understanding the effect of ACAM-J on attention. Higher secondary gradient values in SN during ACAM-J suggest that ACAM-J may enhance attentional resources by redirecting these resources toward a different experiential dimension via the SN. Our neurophenomenological findings support this argument, showing negative correlations between secondary gradient values in VN and the intensity of ACAM-J and positive correlations between secondary gradient values in SN and the intensity of ACAM-J. Similar to the principal gradient findings, correlations with phenomenological attributes were not corrected for multiple comparisons. Therefore, these findings serve as a foundation for future studies to confirm and expand upon the relationships observed in this study.

Together, our findings for the secondary gradient align with descriptions from meditators, who often express a detachment from the external environment during ACAM-J and a decrease in awareness of sensory stimuli (Gunaratana 1988). Notably, the secondary gradient findings also reveal significant differences between ACAM-J and both control conditions. While findings from the principal gradient suggest similarities between the memory condition and ACAM-J, a deeper investigation into the secondary gradient reveals clear differences, particularly in the dissociation of attention- and sensory-related areas. This finding highlights the importance of including both control conditions to provide a detailed understanding of functional reorganization of brain hierarchy during ACAM-J.

There are multiple strengths of our study; it is the first study to apply gradient analysis for investigation of ACAM-J. Furthermore, it is one of the very few ACAM-J studies to date that integrates phenomenological analysis with brain imaging results. We also intensively sampled ACAM-J over 27 times to provide reliable estimation of neural activity and connectivity during ACAM-J (Ganesan et al. 2024). Not withholding these strengths, there are several limitations to the current study that should be considered. First, it is based on a single-case participant design, which inherently restricts the generalizability of the results and is the main limitation of this study. Reliance on a single participant raises the possibility that the observed patterns reflect individual-specific characteristics rather than general mechanisms of ACAM-J. It is also important to note that advanced ACAM-J practitioners are rare, and their ability to reliably signal transitions between meditative states is essential for studies of this nature. Nevertheless, the findings of the study, particularly the alignment between the participant's phenomenological reports with changes observed in functional organization of the brain during ACAM-J, underscore the value of this study and highlight the necessity for future research involving multiple participants to validate and extend these findings. Second, as mentioned previously, the participant reported involuntarily experiencing meditative states during the initial trials of both control conditions. Although, this was observed with reduced intensity compared to the ACAM-J. To assess the impact of reported low-level meditative phenomenology during the control conditions, we conducted a supplementary analysis excluding the initial runs where the participant reported entering a meditative state. The results were consistent with our main findings (see Figs. S1 and S2), supporting the robustness of our conclusions. Given the minimal effect of excluding these runs, all runs were kept in the final analyses. Based on these observations, future studies could consider naturalistic stimuli, such as movie viewing, as a control condition to provide an engaging task that better mirrors real-world dynamics, offering a stronger basis for comparing neural changes during ACAM-J. Furthermore, a possible future direction could involve designing a study that allows for regressing out task-related neural activity to improve the reliability of contrasts between control conditions and ACAM-J states. Third, there was a methodological limitation that prevented us from separately analyzing ACAM-J6 to ACAM-J-8. The nature of these ACAM-J states is such that any attempt by the participant to physically engage, such as pressing a button, may interrupt the state. Consequently, ACAM-J6 to ACAM-J8 were collectively analyzed, which, while limiting in scope, still provided valuable insights into the combined characteristics of these ACAM-J states. While we had to merge ACAM-J6–8 together, this approach did not impact the understanding of the broader phenomenological and neurological aspects of ACAM-J. This is because the most notable phenomenological differences are observed between the initial four ACAM-J and the final four ACAM-J. Finally, segmentation applied to the control runs was another limitation of this study. To ensure enough runs for comparison with the 2-min ACAM-J runs, control runs were divided into 1-min segments. Using 2-min segments for the control conditions would have significantly reduced the number of data points, compromising the robustness of the analysis and limiting statistical comparisons across conditions. To further assess the impact of this segmentation approach, we conducted a supplementary analysis in which the control runs were instead divided into 2-min segments. We reran both the network-level and ROI-level analyses with the revised segmentation of control runs and found that the key findings were largely consistent with those in the main analysis. These supplementary analyses are available in the Figs. S3 and S4. Nonetheless, we acknowledge that segmentation choices can influence functional connectivity estimates, as the number of time points directly affects their reliability. In general, longer scan durations tend to produce more stable estimates (Birn et al. 2013; Hutchison et al. 2013). Future studies could address this by collecting longer control runs, allowing for segmentation strategies that better align with the natural durations of ACAM-J states.

In conclusion, our study highlights the impact of ACAM-J on the hierarchical reorganization of the brain as revealed through gradients' analysis. We demonstrated that ACAM-J induces a significant shift in the macroscale organization of the brain, transitioning from a segregated brain state to a more globally integrated configuration. Additionally, ACAM-J appears to separate connectivity patterns in sensory-related areas from attention modulation-related areas, thereby increasing the differentiation

between primary sensory areas and those involved in attention modulation. These findings not only enhance our understanding of the brain during advanced meditation but also offer opportunities for further research into its long-term effects, safe practice (Wright et al. 2024), and the potential therapeutic applications of advanced meditation.

Author contributions

Umay Demir (Formal analysis, Visualization, Writing—original draft, Writing—review & editing), Winson Fu Zun Yang (Supervision, Writing—review & editing), and Matthew D. Sacchet (Conceptualization, Funding acquisition, Investigation, Methodology, Project administration, Resources, Supervision, Writing—review & editing).

Supplementary material

Supplementary material is available at *Cerebral Cortex* online.

Funding

Dr Sacchet and the Meditation Research Program are supported by the National Institute of Mental Health (Project Number R01MH125850), Dimension Giving Fund, Ad Astra Chandaria Foundation, Brain and Behavior Research Foundation (Grant Number 28972), BIAL Foundation (Grant Number 099/2020), and individual donors.

Conflict of interest statement: We have no competing interests to declare.

Ethics approval statement

The Mass General Brigham IRB approved the study (2019P003902) and the participant provided informed consent.

References

Amaro A. 2021. Realization is here and now. *Mindfulness*. 12:795–797. https://doi.org/10.1007/s12671-020-01526-z.

Anālayo B. 2021. The four levels of awakening. *Mindfulness*. 12: 831–840. https://doi.org/10.1007/s12671-020-01530-3.

Bernhardt BC, Smallwood J, Keilholz S, Margulies DS. 2022. Gradients in brain organization. *NeuroImage*. 251:118987. https://doi.org/10.1016/j.neuroimage.2022.118987.

RAI B et al. 2020. Dispersion of functional gradients across the adult lifespan. *NeuroImage*. 222:117299. https://doi.org/10.1016/j.neuroimage.2020.117299.

Birn RM, Molloy EK, Patriat R, Parker T et al. 2013. The effect of scan length on the reliability of resting-state fMRI connectivity estimates. *NeuroImage*. 83:550–558. https://doi.org/10.1016/j.neuroimage.2013.05.099.

Brasington L. 2015. *Right concentration: a practical guide to the Jhanas*. Boulder, Colorado: Shambhala Publications.

Cahn BR, Delorme A, Polich J. 2010. Occipital gamma activation during vipassana meditation. *Cogn Process*. 11:39–56. https://doi.org/10.1007/s10339-009-0352-1.

Carhart-Harris RL et al. 2014. The entropic brain: a theory of conscious states informed by neuroimaging research with psychedelic drugs. *Front Hum Neurosci*. 8. https://doi.org/10.3389/fnhum.2014.00020.

Centanni SW, Janes AC, Haggerty DL, Atwood B, Hopf FW. 2021. Better living through understanding the insula: why subregions can make all the difference. *Neuropharmacology*. 198:108765. https://doi.org/10.1016/j.neuropharm.2021.108765.

Chowdhury A et al. 2023. Investigation of advanced mindfulness meditation "cessation" experiences using EEG spectral analysis in an intensively sampled case study. *Neuropsychologia*. 190:108694. https://doi.org/10.1016/j.neuropsychologia.2023.108694.

Christopher L et al. 2015. Salience network and parahippocampal dopamine dysfunction in memory-impaired Parkinson disease. *Ann Neurol*. 77:269–280. https://doi.org/10.1002/ana.24323.

Coifman RR, Lafon S. 2006. Diffusion maps. *Appl Comput Harmon Anal*. 21:5–30. https://doi.org/10.1016/j.acha.2006.04.006.

Dong D et al. 2023. Compressed sensorimotor-to-transmodal hierarchical organization in schizophrenia. *Psychol Med*. 53:771–784. https://doi.org/10.1017/S0033291721002129.

Favila SE, Kuhl BA, Winawer J. 2022. Perception and memory have distinct spatial tuning properties in human visual cortex. *Nat Commun*. 13:5864. https://doi.org/10.1038/s41467-022-33161-8.

Fisher NE. 2022. Flavors of ecstasy: states of absorption in Islamic and Jewish contemplative traditions. *Religions*. 13:935. https://doi.org/10.3390/rel13100935.

Fox MD, Corbetta M, Snyder AZ, Vincent JL, Raichle ME. 2006. Spontaneous neuronal activity distinguishes human dorsal and ventral attention systems. *Proc Natl Acad Sci*. 103:10046–10051. https://doi.org/10.1073/pnas.0604187103.

Galante J et al. 2023. A framework for the empirical investigation of mindfulness meditative development. *Mindfulness*. 14:1054–1067. https://doi.org/10.1007/s12671-023-02113-8.

Ganesan S, Yang WFZ, Chowdhury A, Zalesky A, Sacchet MD. 2024. Within-subject reliability of brain networks during advanced meditation: an intensively sampled 7 tesla MRI case study. *Hum Brain Mapp*. 45:e26666. https://doi.org/10.1002/hbm.26666.

Gazzaley A et al. 2007. Functional interactions between prefrontal and visual association cortex contribute to top-down modulation of visual processing. *Cereb Cortex*. 17:i125–i135. https://doi.org/10.1093/cercor/bhm113.

Girn M et al. 2022. Serotonergic psychedelic drugs LSD and psilocybin reduce the hierarchical differentiation of unimodal and transmodal cortex. *NeuroImage*. 256:119220. https://doi.org/10.1016/j.neuroimage.2022.119220.

Gunaratana MH. 1988. *The Jhanas in Theravada Buddhist meditation*. Sri Lanka: Buddhist Publication Society.

Hagerty MR et al. 2013. Case study of ecstatic meditation: fMRI and EEG evidence of self-stimulating a reward system. *Neural Plast*. 2013:1–12. https://doi.org/10.1155/2013/653572.

Hong S-J et al. 2020. Toward a connectivity gradient-based framework for reproducible biomarker discovery. *NeuroImage*. 223:117322. https://doi.org/10.1016/j.neuroimage.2020.117322.

Hutchison RM, Womelsdorf T, Gati JS, Everling S, Menon RS. 2013. Resting-state networks show dynamic functional connectivity in awake humans and anesthetized macaques. *Hum Brain Mapp*. 34: 2154–2177. https://doi.org/10.1002/hbm.22058.

Hyvärinen A, Oja E. 2000. Independent component analysis: algorithms and applications. *Neural Netw*. 13:411–430. https://doi.org/10.1016/S0893-6080(00)00026-5.

Jiang P et al. 2023. The hierarchical organization of the precuneus captured by functional gradients. *Brain Struct Funct*. 228: 1561–1572. https://doi.org/10.1007/s00429-023-02672-5.

Jolliffe IT. 2002. *Principal component analysis*. 2nd ed. [Nachdr.] ed. New York Berlin Heidelberg: Springer, (Springer series in statistics).

Laukkonen RE, Sacchet MD, Barendregt H, Devaney KJ, Chowdhury A, Slagter HA. 2023. *Cessations of consciousness in meditation: advancing a scientific understanding of nirodha samāpatti. In: progress in brain research*. Elsevier. p. S0079612322001984. https://linkinghub.elsevier.com/retrieve/pii/S0079612322001984.

Louchakova-Schwartz O. 2011. The self and the world: Vedanta, Sufism, and the Presocratics in a phenomenological view. In: Tymieniecka A-T, editor. *Phenomenology/Ontopoiesis retrieving geocosmic horizons of antiquity*. Dordrecht: Springer Netherlands. p. 423–438. https://doi.org/10.1007/978-94-007-1691-9_33.

Margulies DS et al. 2016. Situating the default-mode network along a principal gradient of macroscale cortical organization. *Proc Natl Acad Sci*. 113:12574–12579. https://doi.org/10.1073/pnas.1608282113.

Menon V, Uddin LQ. 2010. Saliency, switching, attention and control: a network model of insula function. *Brain Struct Funct*. 214: 655–667. https://doi.org/10.1007/s00429-010-0262-0.

Metzinger T. 2020. Minimal phenomenal experience: meditation, tonic alertness, and the phenomenology of "pure" consciousness. *Philos Mind Sci*. 1:1–44. https://doi.org/10.33735/phimisci.2020.I.46.

Millière R, Carhart-Harris RL, Roseman L, Trautwein F-M, Berkovich-Ohana A. 2018. Psychedelics, meditation, and self-consciousness. *Front Psychol*. 9:1475. https://doi.org/10.3389/fpsyg.2018.01475.

Park B et al. 2022. Multiscale neural gradients reflect transdiagnostic effects of major psychiatric conditions on cortical morphology. *Commun Biol*. 5:1024. https://doi.org/10.1038/s42003-022-03963-z.

Preller KH et al. 2017. The fabric of meaning and subjective effects in LSD-induced states depend on serotonin 2A receptor activation. *Curr Biol*. 27:451–457. https://doi.org/10.1016/j.cub.2016.12.030.

Raut RV, Snyder AZ, Raichle ME. 2020. Hierarchical dynamics as a macroscopic organizing principle of the human brain. *Proc Natl Acad Sci*. 117:20890–20897. https://doi.org/10.1073/pnas.2003383117.

Sacchet MD, Fava M, Garland EL. 2024. Modulating self-referential processing through meditation and psychedelics: is scientific investigation of self-transcendence clinically relevant? *World Psychiatry*. 23:298–299. https://doi.org/10.1002/wps.21214.

Sayadaw P. 2008. *Knowing and seeing*. Pa-Auk Meditation Centre, Singapore: Free Distribution.

Schaefer A et al. 2018. Local-global parcellation of the human cerebral cortex from intrinsic functional connectivity MRI. *Cereb Cortex*. 28:3095–3114. https://doi.org/10.1093/cercor/bhx179.

Schober P, Boer C, Schwarte LA. 2018. Correlation coefficients: appropriate use and interpretation. *Anesth Analg*. 126:1763–1768. https://doi.org/10.1213/ANE.0000000000002864.

Sezer I, Pizzagalli DA, Sacchet MD. 2022. Resting-state fMRI functional connectivity and mindfulness in clinical and non-clinical contexts: a review and synthesis. *Neurosci Biobehav Rev*. 135:104583. https://doi.org/10.1016/j.neubiorev.2022.104583.

Shankman R. 2008. *The experience of Samadhi: an in-depth exploration of Buddhist meditation*. Boulder, Colorado: Shambhala Publications.

Smallwood J et al. 2021. The default mode network in cognition: a topographical perspective. *Nat Rev Neurosci*. 22:503–513. https://doi.org/10.1038/s41583-021-00474-4.

Smith RA et al. 2006. Antisense oligonucleotide therapy for neurodegenerative disease. *J Clin Invest*. 116:2290–2296. https://doi.org/10.1172/JCI25424.

Sparby T, Sacchet MD. 2022. Defining meditation: foundations for an activity-based phenomenological classification system. *Front Psychol*. 12:795077. https://doi.org/10.3389/fpsyg.2021.795077.

Sparby T, Sacchet MD. 2024. Toward a unified account of advanced concentrative absorption meditation: a systematic definition and classification of Jhāna. *Mindfulness*. 15:1375–1394. https://doi.org/10.1007/s12671-024-02367-w.

Studerus E, Kometer M, Hasler F, Vollenweider FX. 2011. Acute, subacute and long-term subjective effects of psilocybin in healthy humans: a pooled analysis of experimental studies. *J Psychopharmacol*. 25:1434–1452. https://doi.org/10.1177/0269881110382466.

Taylor VA et al. 2013. Impact of meditation training on the default mode network during a restful state. *Soc Cogn Affect Neurosci*. 8: 4–14. https://doi.org/10.1093/scan/nsr087.

Timmermann C et al. 2023. Human brain effects of DMT assessed via EEG-fMRI. *Proc Natl Acad Sci*. 120:e2218949120. https://doi.org/10.1073/pnas.2218949120.

Uddin LQ. 2015. Salience processing and insular cortical function and dysfunction. *Nat Rev Neurosci*. 16:55–61. https://doi.org/10.1038/nrn3857.

Van Lutterveld R, Chowdhury A, Ingram DM, Sacchet MD. 2024. Neurophenomenological investigation of mindfulness meditation "cessation" experiences using EEG network analysis in an intensively sampled adept meditator. *Brain Topogr*. 37:849–858. https://doi.org/10.1007/s10548-024-01052-4.

Venkatesh S, Raju TR, Shivani Y, Tompkins G, Meti BL. 1997. A study of structure of phenomenology of consciousness in meditative and non-meditative states. *Indian J Physiol Pharmacol*. 41: 149–153.

Vos De Wael R et al. 2020. BrainSpace: a toolbox for the analysis of macroscale gradients in neuroimaging and connectomics datasets. *Commun Biol*. 3:103. https://doi.org/10.1038/s42003-020-0794-7.

Wagstyl K, Ronan L, Goodyer IM, Fletcher PC. 2015. Cortical thickness gradients in structural hierarchies. *NeuroImage*. 111:241–250. https://doi.org/10.1016/j.neuroimage.2015.02.036.

Wright MJ, Sanguinetti JL, Young S, Sacchet MD. 2023. Uniting contemplative theory and scientific investigation: toward a comprehensive model of the mind. *Mindfulness*. 14:1088–1101. https://doi.org/10.1007/s12671-023-02101-y.

Wright MJ et al. 2024. Altered states of consciousness are prevalent and insufficiently supported clinically: a population survey. *Mindfulness*. 15:1162–1175. https://doi.org/10.1007/s12671-024-02356-z.

Xia M et al. 2022. Connectome gradient dysfunction in major depression and its association with gene expression profiles and treatment outcomes. *Mol Psychiatry*. 27:1384–1393. https://doi.org/10.1038/s41380-022-01519-5.

Yang WFZ et al. 2024a. Intensive whole-brain 7T MRI case study of volitional control of brain activity in deep absorptive meditation states. *Cereb Cortex*. 34:bhad408. https://doi.org/10.1093/cercor/bhad408.

Yang WFZ, Sparby T, Wright M, Kim E, Sacchet MD. 2024b. Volitional mental absorption in meditation: toward a scientific understanding of advanced concentrative absorption meditation and the case of jhana. *Heliyon*. 10:e31223. https://doi.org/10.1016/j.heliyon.2024.e31223.

Yeager BE et al. 2022. Central precuneus lesions are associated with impaired executive function. *Brain Struct Funct*. 227:3099–3108. https://doi.org/10.1007/s00429-022-02556-0.

Yeo BT et al. 2011. The organization of the human cerebral cortex estimated by intrinsic functional connectivity. *J Neurophysiol*. 106: 1125–1165. https://doi.org/10.1152/jn.00338.2011.

Zhang J et al. 2019. Intrinsic functional connectivity is organized as three interdependent gradients. *Sci Rep*. 9:15976. https://doi.org/10.1038/s41598-019-51793-7.

Cerebral Cortex, 2025, **35**, bhaf079
https://doi.org/10.1093/cercor/bhaf079
Original Article